

Title Page

Human Metabolism of Lapatinib, a Dual Kinase Inhibitor: Implications for Hepatotoxicity

Stephen Castellino, Michael O'Mara, Kevin Koch, David J Borts, Gary D Bowers,

Christopher MacLauchlin

Department of Drug Metabolism and Pharmacokinetics, GlaxoSmithKline RTP, NC (SC,
MO, GDB, CM)

Department of Clinical Pharmacokinetics, GlaxoSmithKline RTP, NC (KK)

Field Analytics, BASF Plant Science, Ames, IA (DJB)

Running Title Page

Running Title:

Human Metabolism of Lapatinib: Hepatotoxicity Implications

Corresponding Author:

Stephen Castellino

GlaxoSmithKline
5 Moore Dr.
RTP, NC 27709

steve.x.castellino@gsk.com

919-483-2262

Number of text pages: 46

Number of tables: 4

Number of figures and schemata: 10

Number of references: 31

Number of words – abstract: 206

Number of words – introduction: 618

Number of words – discussion: 1589

Nonstandard Abbreviations: ErbB, epidermal growth factor receptor; HER2, human epidermal growth factor receptor 2; ATP, Adenosine-5'-triphosphate; DILI, drug induced liver injury; HLA-DQA1, major histocompatibility complex, class II, DQ alpha 1; ALT, alanine aminotransferase; CYP, cytochrome P450; LSC liquid scintillation counting; EIC, extracted ion chromatogram; BQL, below the limit of quantification; AST, aspartate aminotransferase

Abstract

Lapatinib (Tykerb/Tyverb) is an important orally active dual tyrosine kinase inhibitor efficacious in combination therapy for patients with progressive HER2-overexpressing metastatic breast cancer. However, clinically significant liver injury has been reported which may be associated with lapatinib metabolic activation. We describe the metabolism and excretion of [^{14}C]-lapatinib in six healthy human volunteers following a single oral dose of 250 mg and the potential relationships between metabolism and clinical hepatotoxicity. Overall, elimination showed high inter-subject variability, with fecal elimination being the predominant pathway representing a median of 92% of the dose with lapatinib as the largest component (ca. median 27% dose). In plasma, approximately 50% of the observed radioactivity was attributed to metabolites. Analysis of a 4 hour pooled plasma extract identified seven metabolites related by an N- and α -carbon oxidation cascade and oxidation. Fecal metabolites derived from three prominent pathways: N- and α -carbon oxidation, fluorobenzyl oxidative cleavage, and hydroxypyridine formation. Undoubtedly, several of the lapatinib metabolites can be linked to reactive species such as aldehydes or quinone imines. In addition to the contribution of these potentially reactive metabolites as suspects in clinical liver injury, the role of other disposition factors, including interaction with drug transporters, pharmacogenetics, or magnitude of the therapeutic dose, should not be discounted.

Introduction

Lapatinib (Tykerb/Tyverb; GlaxoSmithKline) is an orally active dual tyrosine kinase inhibitor of the epidermal growth factor receptor 1 (ErbB1) and human epidermal receptor 2 (HER2). The ErbB1 and HER2 transmembrane tyrosine kinase receptors are signaling proteins implicated in the pathogenesis of breast cancer that regulate cellular growth, proliferation, survival and differentiation. Increased expression and activation of HER2, reported in approximately 20% of human breast cancers, is associated with a higher risk for recurrence of breast cancer and a poorer clinical outcome. Lapatinib acts intracellularly by reversibly binding to the cytoplasmic ATP-binding site of the kinase, preventing receptor phosphorylation and activation. Simultaneous inhibition of both ErbB1 and HER2 is an appealing therapeutic strategy compared with agents that inhibit ErbB1 or HER2 alone. Currently, lapatinib is used in combination with capecitabine or letrozole in patients with progressive HER2-overexpressing metastatic breast cancer previously treated with an anthracycline, a taxane and trastuzumab with efficacious doses at 1250 or 1500 mg QD (Boyd et al., 2005; Johnston & Leary, 2006; Moy & Goss, 2006, Geyer et al., 2006).

Lapatinib has an acceptable safety profile for the treatment of breast cancer (Geyer et al., 2006). However, serious drug induced liver injury (DILI) of cancer patients receiving lapatinib has been reported (Moy et al., 2009). Hepatotoxicity has also been reported for other tyrosine kinase inhibitors including imatinib and metabolic activation has been suggested as an underlying factor (Loriot et al., 2008, Duckett & Cameron, 2010).

In the case of the tyrosine kinase inhibitor CP-724,714, direct mitochondrial toxicity and inhibition of bile salt efflux are reported to contribute to hepatotoxicity (Feng et al., 2009). Recently, a clinical pharmacogenetic investigation of lapatinib patients reported a significant association between the major histocompatibility complex HLA-DQA1*02:01 and ALT elevation (Spraggs et al., 2011). Associations between DILI and specific HLA polymorphisms have been observed for other drugs as well such as amoxicillin-clavulanate, flucloxacillin, ximelagatran, and ticlopidine (Russmann et al., 2010). Furthermore, DILI occurs at a higher frequency in compounds that have 50% or greater hepatic metabolism, (Chalasanani & Bjornsson, 2010) suggesting an important role for metabolites in hepatotoxicity. For lapatinib, the underlying mechanism of hepatotoxicity has not been fully elucidated, however, it is possible that a combination of factors, rather than a single component, may ultimately be responsible.

Lapatinib absorption is incomplete and variable following oral administration and systemic exposure is increased when administered with food (Koch et al., 2007) with likely associated increases in hepatic exposures to lapatinib and its metabolites. Lapatinib undergoes extensive metabolism, primarily by CYP3A4 and CYP3A5, with minor contributions from CYP2C19 and CYP2C8 to a variety of oxidized metabolites. Recent *in vitro* experiments with lapatinib have shown that CYP mediated O-dealkylation resulted in a phenol metabolite where further oxidation of the phenol could result in the formation of a quinone imine, capable of reacting with cellular proteins or glutathione (Teng et al., 2010). Para-hydroxyaniline metabolites are also formed from the metabolism of other kinase inhibitors, dasatinib, gefitinib and erlotinib (Duckett and Cameron, 2010). Lapatinib is known to be a substrate and inhibitor for the transporters

breast cancer resistance protein (BCRP, ABCG2) and P-glycoprotein (P-gp, ABCB1) *in vitro* and inhibits the hepatic uptake transporter OATP 1B1, at clinically relevant concentrations *in vitro* (Polli et al., 2008). It is therefore possible that lapatinib, or its metabolites, has the potential to inhibit other relevant hepatic transporters such as the bile salt efflux pump (BSEP).

Further insights into the mechanism of hepatotoxicity rely on understanding the human metabolism of lapatinib. Thus, we report our findings from a study of the metabolism and excretion of [¹⁴C]-lapatinib in healthy human volunteers after administration of a single oral dose of 250 mg and the potential relationships between the metabolites of lapatinib and observed clinical hepatotoxicity.

Materials and Methods

Materials. [¹⁴C]-lapatinib (GW572016), was prepared and analyzed by Isotope Chemistry, Chemical Development, GSK, Stevenage, UK (Figure 1). Analytical purity was determined as 99.6% (w/w), and radiochemical purity (HPLC) was determined as greater than 99%. The specific activity of the lapatinib ditosylate monohydrate salt was 8.13 kBq/mg (0.22 μCi/mg). Authentic standards of metabolites: M1, M4, M5, M11, and M12 were supplied by Pharmaceutical Development or Chemical Development, GlaxoSmithKline, and were used as reference standards for chromatography, mass

spectrometry, or NMR. All other chemicals used during this study were reagent grade or better, and were obtained from standard chemical suppliers.

Formulated Drug. A mixture of unlabeled lapatinib and [^{14}C]-lapatinib, equivalent to 250 mg lapatinib free base (containing 89.1 μCi of [^{14}C]-radioactivity), was dosed to each subject as an aqueous suspension (total volume of 80 ml of water). The specific activity of the dose measured as free base was calculated to be 0.356 $\mu\text{Ci}/\text{mg}$

Clinical Mass Balance Study Design. The clinical portion of this study was conducted by Covance Laboratories Inc. (Covance, Madison, WI), in accordance with Good Clinical Practice (GCP) guidelines, the guiding principles of the Declaration of Helsinki, Covance standard operating procedures (SOPs), the Nuclear Regulatory Commission (NRC) regulations, and all applicable subject privacy requirements. All subjects provided written informed consent before participation.

This was an open-label, single-dose, mass balance study in six healthy male or female subjects to determine the metabolic profile and routes of excretion of lapatinib in humans. Subject demographics consisted of three males and three females (all of non-child-bearing potential), with four subjects African-American and two Caucasian. The median subject age was 44.5 years (range: 18-49 years), with a height of 171.5 cm (143-183 cm), and a weight of 73.8 kg (58.9-86.8 kg), with body mass index (BMI) of 26.08 kg/m^2 (23.9-29.7 kg/m^2). Lapatinib was well tolerated with no clinically significant changes in clinical laboratory values, vital sign parameters, or serious adverse events. No concomitant medications were reported in this study.

Subjects were admitted to the clinical research unit on the evening before the dosing day and remained there until all samples were collected for a total of 7 days and 8 nights. A 250 mg dose of [¹⁴C]-lapatinib was administered as an oral suspension to each subject and blood, urine, and fecal samples were collected predose and for 168 hours postdose for pharmacokinetic analyses and metabolic profiling. The total time a subject was on study was 38 days. Subjects were required to fast from 10 hours predose until approximately 4 hours postdose. Water was allowed freely, except for 1 hour predose until 2 hours postdose.

Blood was collected via the antecubital intravenous cannula predose and for 168 hours postdose. During the study period, a total of 24 blood samples (15 ml each) were collected at the following times for pharmacokinetic analysis: predose, 0.25, 0.5, 1, 1.5, 2, 2.5, 3, 4, 6, 8, 10, 12, 16, 24, 36, 48, 60, 72, 84, 96, 120, 144, and 168 hours postdose. Blood samples were collected into glass collection tubes containing K₃-ethylenediamine tetraacetic acid (15 ml total collected in a 3-, 5-, and 7-ml tubes). The sample was mixed and centrifuged at approximately 1000x g for 10 to 15 minutes. The resulting plasma was transferred to appropriately labeled polypropylene storage tubes for analysis of lapatinib (1 ml), total radioactivity (2 ml), and metabolite profiling (3 ml), and stored in an upright position at or below -20 °C until analyzed.

Urine was collected predose and for 168 hours postdose for pharmacokinetic analysis. A total of 10 urine samples was collected for pharmacokinetic analysis during the following intervals: predose, and between 0 to 4, 4 to 8, 8 to 12, 12 to 24, 24 to 48, 48 to 72, 72 to

96, 96 to 120, 120 to 144, and 144 to 168 hours postdose. All urine produced by a subject during each collection interval was combined and stored in a sterile plastic container in a refrigerator set at 2 to 8 °C. A 25-ml aliquot of each combined urine sample was transferred into a prelabeled polypropylene storage container and then stored in an upright position at or below -20 °C until analyzed.

Feces were collected predose and for 168 hours postdose for pharmacokinetic analysis. Each fecal sample collection was weighed and placed in a prelabeled, sealable container in an upright position at or below -20 °C until analyzed.

Quantification of Lapatinib in Plasma. Concentrations of lapatinib in plasma samples were determined with a validated analytical method, over the range 5 to 5000 ng/ml, by LC/MS/MS. Lapatinib was extracted from 25 µl of human plasma by protein precipitation using 80:20 (v:v) acetonitrile:10 mM ammonium acetate (pH 4.5) containing an isotopically labeled internal standard ($[^2\text{H}_3\ ^{15}\text{N}_1\ ^{13}\text{C}_2]$ -GW572016). Extracts (2 µl) were injected onto a Hypersil-Keystone Fluophase PFP column (50x2.1mm, Thermo Scientific), maintained at 40 °C and eluted isocratically by using 10 mM ammonium acetate (pH 4.5):acetonitrile:water (20:70:10) at a flow rate of 0.65 ml/min. Detection was performed by positive ion MS/MS using a TurboIonSpray™ interface on an API-4000 mass spectrometer (Applied Biosystems; Framingham, MA) with multiple reaction monitoring (m/z 581 - m/z 365 for lapatinib and m/z 587 – m/z 367 for the internal standard).

Radioanalytical Methods. All fecal sample combustions were performed in a Model 307 Sample Oxidizer (Packard Instrument Company; Downers Grove, IL). The resulting $^{14}\text{CO}_2$ was trapped in Carbo-Sorb. Perma-Fluor scintillation cocktail and the radioactivity content were quantified by Liquid Scintillation Counting (LSC). All samples, including plasma and urine, were directly counted by LSC by using Ultima Gold scintillation cocktail. The samples were counted in a Model 1900TR or 2300TR liquid scintillation counter (Packard) for at least 5 min or 100,000 counts. The LSC data (counts per minute; cpm) were automatically corrected for counting efficiency by using an external standardization technique and an instrument-stored quench curve generated from a series of sealed quenched standards to obtain disintegrations per minute (dpm). The LSC data were corrected for background by subtracting the dpm value measured from the analysis of a blank sample. Plasma and urine samples were thawed, homogenized and triplicate weighed aliquots from each postdose sample (*ca.* 0.2 g each) were submitted for radioanalysis. The fecal samples were thawed, mixed with water (enough to create a slurry) and the total weight recorded. The samples were homogenized with a probe-type homogenizer and triplicate weighed aliquots (*ca.* 0.2 g each) were combusted and analyzed for radioactivity. If results for sample replicates (calculated as dpm/g or dpm/ml sample, as applicable) differed by more than 10% from the mean value, the sample was re-homogenized (where appropriate) and reanalyzed. This specification was met for all sample aliquots that had radioactivity greater than 500 dpm.

Metabolite Radiochemical Profiling. The radiochemical profiles of [^{14}C]-lapatinib-derived radioactivity were determined for selected fecal homogenate and plasma extracts by using HPLC combined with radiochemical flow detection or fractionation and off-line

counting. HPLC-radiometric data were generated on-line by using a Packard 500TR series flow scintillation analyser and Packard Ultima Flo M scintillation fluid (Ultima-Flo-M; Packard, Downers Grove, IL) with a scintillant flow rate of 1 ml/min. For off-line analysis, representative fecal homogenate and plasma extracts were fractionated into 96-well plates by using HPLC. A portion of each fraction was transferred to a separate 96-well plate and combined with scintillation cocktail for liquid scintillation counting. Reconstructed radiochemical profiles were compiled from the resulting data. Plates containing the original fecal homogenate, plasma extract fractions and other selected samples were analyzed by using nanoelectrospray/MS. Off-line radiodetection was performed with either a Wallac 1450 Microbeta liquid scintillation analyzer or a Packard Tricarb 2500TR liquid scintillation counter. Liquid scintillant was added at 150 μ l/well (Ultima Flo-M; Packard). Data tables (radioactivity concentration and percentage of dose) were generated by DEBRA, Version 5.2a (LabLogic; South Yorkshire, UK), an automated and validated data capture and management system for studies using radiolabeled test material.

Four plasma pools were prepared for extraction. Three pools were used to generate LC-radiochemical profiles, while the fourth pool was used for LC/MS analysis. The first pool contained equal volumes of 4-hour postdose plasma from all six subjects. The second pool contained equal volumes of 3-, 4- and 6-hour postdose plasma from a single female subject. The third pool contained equal volumes of 2.5-, 3- and 8-hour postdose plasma from 3 male subjects. The fourth pool contained equal volumes of 1.5-, 2-, 3-, 4- and 6-hour postdose plasma from a different female subject. In all cases, one volume of

human plasma was extracted with two volumes of methanol and two volumes of acetonitrile. The extract was vigorously mixed to a vortex followed by centrifugation for approximately 5 minutes. The supernatant was removed and the volume reduced to approximately 0.1 ml under either a stream of nitrogen at ambient temperature or reduced to dryness overnight using a Savant Speedvac on the low drying setting. The dried extract was reconstituted with 100 μ L of the starting mobile phase for the method. Approximately 90 μ L of sample extract was injected onto the HPLC column.

Due to the limited amount of radiocarbon associated with many of the plasma samples, analyses were conducted by using HPLC with fraction collection followed by liquid scintillation counting. Fractions collected from the analysis of human plasma produced an average background of approximately 9 dpm when using the Wallac 1450 Microbeta liquid scintillation analyzer. A 3:1 signal to noise ratio (27 dpm or approximately 23 ng-equivalents) was chosen as the limit of quantitation for off-line liquid scintillation counting.

HPLC method 1 (used for analysis of plasma). The chromatographic system was comprised of an Agilent 1100 binary pump (Agilent, Santa Clara) and autosampler, manual fraction collection, column oven (45 °C), UV detector (λ 277 nm), and Waters Symmetry C18 column (4.6 mm x 150 mm, 5 μ m). The mobile phase consisted of water:formic acid (0.1% v:v) (Solvent A) and methanol:acetonitrile (10 mM ammonium acetate, pH=4.5, 72:23:5 v:v:v) (Solvent B). A flow rate of 1 ml/min was maintained for

the entire run. The following 90 min linear gradient was used: start at 15% B for 10 min, increase to 35% B over 20 min, increase to 50% B over 10 min, increase to 60% B over 10 min, increase to 75% over 10 min and an increase to 90% B over 5 min. The column was re-equilibrated after each injection. HPLC column recoveries were determined for selected samples by collecting the total HPLC columns eluate, determining the total amount of radioactivity recovered and comparing that with the amount of radioactivity injected onto the column.

HPLC method 2 (used for analysis of plasma to resolve N-oxidation products).

Chromatographic system and column were the same as method 1. The mobile phase consisted of water:formic acid (0.1% v:v) (Solvent A) and acetonitrile containing 0.1% formic acid (v/v) (Solvent B). A flow rate of 1 ml/min was maintained for the entire run. The following 90 min linear gradient was used: start at 27% B and hold for 5 min, increase to 28% B over 5 min, increase to 38% B over 20 min, and increase to 90% B over 2 min. The column was re-equilibrated after each injection.

For fecal radiochemical profiles, time points were selected for each subject such that at least 90% of the total radioactivity over the sample collection period was represented. Approximately 1 to 5 grams of each selected fecal homogenate were extracted (liquid-liquid) with ethanol:acetonitrile:sample (3:3:1/v:v:v). The extraction vessels were mixed to a vortex, shaken for approximately 1 hour, the supernatant removed and reduced to dryness with a Savant Speedvac. The dried extract was reconstituted with DMSO:methanol:acetonitrile (2:1:1/v:v:v) prior to HPLC analysis. Selected fecal

homogenates, representing >90% of the radiocarbon recovered in feces for each subject, were analyzed by HPLC-radio profiling method 1. No urine samples were analyzed by HPLC due to the low percentage of the dose (median 1.2%) recovered in the urine.

Identification of Metabolites. Structural characterization by mass spectrometry (MS) was performed using selected sample isolates by nanoelectrospray infusion on a Q-ToF MS (Waters; Beverly, MA) operating in positive ion mode. Collision energies were ramped between 20-40 eV and the optimum energy for each metabolite was selected. Leucine enkephalin (2µg/ml) was spiked into the sample at 10% (v/v). Lapatinib metabolites were characterized by the accurate mass measurement of the full scan protonated molecular ion and collision-induced dissociation (CID) fragmentation. All human lapatinib metabolites had previously been fully characterized by MS and NMR from preclinical studies or synthesis. Synthetic standards were used for comparison of chromatographic retention times as well as characteristic MS fragmentation patterns. Analytical reference data are included in Table 4.

Analysis and identification of drug-related material in human plasma were also performed by using LC/MS with HPLC method 1. This system consisted of an Agilent 1100 binary pump, autosampler, column oven (45 °C), and UV detector (λ 277 nm) interfaced with a Sciex API-150 (Applied Biosystems; Framingham, MA) single quadrupole mass spectrometer with an electrospray ion source (positive ion) operated in full scan mode (m/z 100 to 900). Chromatographic retention times and protonated

molecular ions (m/z) were used with synthetic standards to characterize lapatinib metabolites.

Results

Pharmacokinetics of Lapatinib and Total Radioactivity

Lapatinib was well tolerated with no clinically significant changes in laboratory values, vital signs, or serious adverse events observed. The median plasma concentration-time profiles and pharmacokinetic parameters of total unchanged lapatinib and radioactivity in healthy volunteers (n=6) after a single 250 mg oral dose of [¹⁴C]-lapatinib are shown in Figure 2 and Table 1, respectively. The median time to reach peak plasma concentration (T_{max}) was approximately 4 h for both lapatinib and total radioactivity. The highest concentrations (C_{max}) in plasma of lapatinib and total radioactivity achieved were 0.33 mg/l (range, 0.15 – 1.07) and 0.72 mg/l (range, 0.40 -1.69), respectively. Radioactivity levels at 24 h were below limits of quantification while lapatinib levels were determined to 72 h post dose.

Mass Balance and Excretion in Urine and Feces

In healthy male and female subjects (n=6) following a single 250 mg oral suspension dose of [¹⁴C]-lapatinib, the median total recovery of radioactivity was 93.1% (range of 61.7 to 99.7%). Two subjects had overall recoveries of 61.7% and 71.5% of the administered radioactivity, while the other four subjects had overall recoveries greater than 90%. The low recovery for these two subjects does not appear to be due to an

inadequate duration of sampling or the analytical methodology and remains unexplained (Roffey et al., 2007). Due to the variability in recovery of total radioactivity, data are best represented by the median. There were no notable differences in mass balance, based on the subject's gender (Table 2). After 48 hours following dose administration, approximately 50% of the total recovered radioactivity was excreted. Fecal excretion was the predominant route of elimination, accounting for a median of 91.8% (range of 60.3 to 98.4%) of the recovered dose. Excretion of radioactivity in feces occurred gradually over 168 h (Table 3). Urinary excretion was minimal (median of 1.16%; range of 0.49% to 1.61%).

Metabolite Profiling and Characterization

Recovery of radioactivity following the extraction of human plasma was determined to be >90%. However, only a single quantifiable LC-radioactive peak, identified as lapatinib by MS analysis, was observed in a multi-subject pooled 4-hour plasma extract (Figure 3). The amount of radioactivity associated with the single peak accounted for approximately half of the total radioactivity extracted from the plasma based on the LC/MS/MS quantitative analysis of lapatinib. It was estimated that the limit of radiochemical quantification, in this chromatogram, was approximately 5% of the total radioactivity of the pooled plasma sample (23 ng equivalents) or approximately 10% of the peak area associated with lapatinib. Various plasma pools consisting of time points from 1.5-8 hours also demonstrated that lapatinib was the only quantifiable radioactive peak present in the chromatogram.

In order to account for the estimated 50% of the radioactivity in the plasma extract that was not quantifiable in the radiochemical chromatogram, LC/MS with a secondary chromatographic method was employed to detect and identify drug related material. Seven metabolites in addition to lapatinib were identified, including a hydroxylamine (M8), two oximes (stereo-isomers, M9; M10), two nitrones (regioisomers, M6; M7), an aldehyde (M11) and a carboxylic acid (M12). These metabolites likely originate from an N-oxidation cascade of the aliphatic secondary amine and may also include contributions from N- α -carbon oxidation (Scheme1). A composite of extracted ion chromatograms (EIC) obtained from the LC/MS analysis of pooled human plasma (female subject, pool 1.5 to 6 hours) following a single oral dose of [^{14}C]-lapatinib is shown in Figure 4. These metabolites, and potentially other metabolites present at low concentrations, appear to represent the majority of the total radioactivity not accounted for by lapatinib. No metabolites containing the chloro-phenol moiety (M1 and M3) were detected in plasma. Additionally, it should be noted that not all of the minor drug related components, observed by LC/MS, were characterized.

The fecal collection periods selected for radiochemical profiling represented 94.7 % (± 2.3) of the dose recovered in the feces. Mean radioactivity extraction efficiencies from the fecal homogenates were 86.2% (± 9.5). The HPLC-radiochemical chromatograms of the fecal homogenates showed a high degree of variability among subjects and were characterized by the presence of a few notable metabolites and many minor metabolites. Of the total 18 radiochemical peaks that were quantifiable in at least one radiochemical profile, only two peaks had a median of greater than 10% of the dose. Representative

HPLC-radiochemical chromatograms of fecal extracts are shown in Figure 5. These two chromatograms contained all of the notable metabolites but demonstrate the variability in the relative proportions of metabolites present.

Lapatinib was present in all fecal homogenates with a median value of 27.0% of the dose; however, the range was between 2.7 and 66.9 %. The subject with the lowest amount of lapatinib (2.7%) also had poor overall recovery of radioactivity (71.5%). Two significant metabolites, M1 and M3, were characterized as oxidative cleavage products resulting in the formation of phenol metabolites. The median value for the phenol, M1, was 3.9% of the dose and ranged from below the limit of quantification (BQL) to 19.2%. M3, a phenol which is also hydroxylated on the quinazoline moiety, constituted a median 3.3% of the dose (range from BQL to 17.8%). The one subject who had values BQL for both M1 and M3 also had poor overall recovery of cumulative radioactivity (61.7%). The carboxylic acid metabolite, M12, was present in the fecal homogenate profiles of all subjects. The median amount of this metabolite was 14.0% (0.4 to 32.5%) and was the only metabolite with a median value greater than 10% of the dose. The most structurally novel metabolite quantified in the fecal homogenates was the intramolecular cyclized hydroxypyridine, M2, related to the pyridinium salt, M5, which was observed as a small partially resolved shoulder of lapatinib in some chromatograms. The median amount of M2 was 6.3% of the dose, ranging from BQL to 14.5%. Other metabolites represented in Scheme 1 were detected by LC/MS in the fecal homogenate but were below the limit of quantification. Evidence of the N-dealkylated metabolite, M4, was also observed by LC/MS.

Discussion

Lapatinib is an orally active dual tyrosine kinase inhibitor of ErbB1 and HER2 currently approved for use in the treatment of breast cancer. Lapatinib has an acceptable safety profile for its therapeutic indication, however, hepatotoxicity (ALT or AST >3 times the upper limit of normal and total bilirubin >2 times the upper limit of normal) has been observed in clinical trials (<1% of patients) and postmarketing experience (GlaxoSmithKline, 2007). Recent advances in molecular toxicology have established a basis for understanding mechanisms of hepatotoxins at the chemical and cellular levels with drug metabolism studies providing a logical framework to link in vitro and whole animal studies to man (Park et al., 2006). Thus, understanding the metabolism and distribution of lapatinib in humans provides a platform to investigate the origins of hepatotoxicity and hypothesis building. The metabolism and excretion of [¹⁴C]-lapatinib were studied in healthy human volunteers, following administration of a single oral dose of 250 mg. This study was conducted at a sub-therapeutic dose; therefore, the relative quantities of metabolites formed may not be reflective of the clinical setting where saturation of biotransformation or transport pathways may occur. Nevertheless, this study provides a key understanding of lapatinib metabolism in humans and further highlights the potential complex relationships between the metabolites and clinical hepatotoxicity.

While some quantitative details of the mass balance and radiochemical profiling were limited by the high degree of variability, an understanding of lapatinib metabolism in humans has emerged. Lapatinib is extensively metabolized, exemplified by diverse

biotransformations to form metabolites, for which many are linked through common pathways. All the metabolites were distributed across all subjects, in feces or plasma, with none of the metabolites, by themselves, consistently accounting for a significant quantity of the administered dose. Three main biotransformation pathways for lapatinib were identified in humans. The first, involves the formation of the phenol moieties by oxidative cleavage of the fluorbenzyl group. These metabolites were observed in feces but were not detected in plasma. In the preclinical species (rat and dog), this pathway predominates with biliary elimination of M1 as both glucuronide and sulfate conjugates accounting for a large portion of the dose (Castellino et al., unpublished observations). Similarly, in humans, biliary excretion of the corresponding conjugates could be anticipated; however, the proportion of the dose cleared by this oxidative cleavage pathway is greatly reduced relative to the preclinical species.

Multiple pathways initiated by N- and α -carbon oxidations may be involved in accounting for the metabolites derived from the secondary amine. Oxidation of the secondary aliphatic nitrogen leads to a hydroxylamine, M8, (Scheme 1). Further oxidation of the hydroxylamine followed by elimination gives rise to two geometric nitron isomers (M6, M7) and represents a branching point in the cascade. Hydrolysis of the Δ -N₇C₈ nitron metabolite, M7, would produce a primary hydroxylamine and methylsulfonyl acetaldehyde. Further oxidation of the hydroxylamine would lead to a nitroso intermediate which tautomerizes to produce the two observed stereomeric oxime isomers (M9; M10). Additionally, hydrolysis of the Δ -N₇C₆ nitron, M6, would result in the corresponding furfuraldehyde metabolite, M11, a potentially reactive electrophilic

intermediate implicated in a similar cascade starting with a piperazine moiety (Rodriguez et al., 1999). A final oxidation step to the corresponding carboxylic acid appears to be the terminal step in the cascade. The carboxylic acid metabolite, M12, was quantitatively the most significant, suggesting that formation of the Δ -N₇C₆ nitron, and α -carbon oxidation at C6 to generate the fufuraldehyde, M11, is the favored pathway.

Spectroscopic evidence for the hydrolysis of nitrones M6 and M7 to the fufuraldehyde, M11, and a primary hydroxylamine, respectively, was obtained from chromatographically isolated nitrones (data not shown).

In addition, α -carbon oxidation pathways could also contribute to the formation of metabolites M9, M10, M11 and M12. The N-dealkylated species, M4, resulting from α -carbon oxidation (C8) to the carbinol amine followed by hydrolysis, was not observed as a major metabolite. However, the observed low levels of M4 could be attributed to its intermediacy in two further biotransformation pathways: 1) oxidation leading to a primary hydroxylamine followed by further oxidation to the nitroso intermediate which tautomerizes to the oximes M9 and M10 and 2) cyclization resulting in M2. Oxidation of the other α -carbon (C6) to generate the carbinol amine followed by elimination can also contribute to the formation of the fufuraldehyde metabolite, M11 (Scheme 1).

The third pathway of significance results in hydroxypyridine, M2, formation, consistent with an initial bioactivation of the dihydrofuran ring followed by intramolecular cyclization involving the secondary amine. Loss of the ethyl sulfone moiety from the pyridinium salt, M5, results in the stable hydroxyl pyridine (Scheme 2). Similarly, M4

could undergo oxidative cyclization to form M2 directly. An alternative mechanism for the formation of the pyridinium salt involves photooxidation (Kuo et al., 1991), through a common dicarbonyl intermediate (Dalvie et al., 2002), (Scheme 3). Experiments with pre-clinical fecal homogenates spiked with lapatinib demonstrated that formation of the pyridinium salt, M5, was proportional to the sample manipulation time under normal laboratory conditions. Thus, M2 and its precursor, M5, may have resulted from metabolism, the isolation process, or a combination of both.

Overall, the data from this study demonstrate that elimination of lapatinib is predominantly metabolic, with the majority of the dose excreted as metabolites in feces. Variability in the extent of metabolism reflects that observed in systemic exposure to lapatinib. Clinically, the metabolism of lapatinib is predominantly mediated by CYP3A as both ketoconazole (CYP3A inhibitor) and carbamazepine (CYP3A inducer) significantly alter lapatinib exposures (Smith et al, 2009).

CYP3A is the predominant CYP in both the intestinal epithelium and liver (Thummel et al., 1997) where it contributes to a large first-pass metabolism of lapatinib. Additionally, there is considerable interindividual variability in expression and activity of CYP3A (Guengerich, 1999). Because of its involvement in the metabolism of lapatinib, differences in CYP3A-mediated metabolism may have important consequences that influence the development of clinical hepatotoxicity that could arise because of different genetic or environmental factors. Several of the lapatinib metabolites could potentially form reactive electrophilic intermediates that could contribute to hepatotoxicity. A recent

in vitro investigation demonstrated that lapatinib (50 μ M) undergoes CYP3A4 and CYP2C8 mediated O-dealkylation to generate M1 as well as the formation of glutathione and cysteinylglycine conjugates (Teng et al., 2010), the latter conjugates being formed from the reaction of glutathione with the putative quinone imine intermediate.

Furthermore, lapatinib was suggested to be a mechanism-based inactivator of CYP3A4, through formation of the quinone imine that covalently modifies the CYP3A4 apoprotein and/or heme moiety. The authors proposed this route as a potential mechanism to explain clinical hepatotoxicity findings (Teng et al., 2010). Another *in vitro* investigation characterized the metabolic intermediate complex formation of CYP3A4 by lapatinib to be quasi irreversible and mediated through metabolites from N-oxidation rather than the quinone imine (Takakusa et al., 2011). These studies provide good insight into highlighting possible mechanisms, however, these elements may only be a part of the process and a better understanding of the underlying complexities is essential to establish a link from *in vitro* experiments to hepatotoxicity (Obach et al., 2008). *In vivo* studies in preclinical species and *in vitro* human investigations suggest that the O-dealkylation product, the phenol (M1), is extensively glucuronidated and sulfated. In the toxicity species (rat and dog), hepatotoxicity was not observed at clinically relevant exposures of lapatinib. Additionally, the predominant metabolic route of elimination favors formation of M1, suggesting an efficient protective mechanism to potentially reactive intermediates. Nevertheless a recent pharmacogenetic analysis of metastatic breast cancer patients experiencing liver injury while taking lapatinib reported a significant association with the major histocompatibility complex HLA-DQA1*02:01 and ALT elevation (Spraggs et al.,

2011). This suggests an activation of the adaptive immune system in a small subset of patients with HLA-DQA1*0201 to cause liver injury. Other drugs have shown similar HLA associations and may be explained due to covalent binding to proteins by the drug itself, or metabolites, to form a hapten, which are recognized by specific HLA proteins resulting in inflammatory tissue damage (Chessman, et al., 2008).

If the lapatinib metabolites are potential suspects in clinical liver injury, interdependency on other disposition factors such as interaction with drug transporters should not be discounted (Scheme 4). In plasma, only metabolites emanating from oxidation of the secondary aliphatic nitrogen or α -carbons appear and only in small quantity. All other metabolites are found in the feces suggesting an efficient biliary elimination route is present with liver exposure being significantly different than what is represented in plasma. The role that transporters have in the disposition and drug interactions of lapatinib have been well characterized (Polli et al., 2008) and it is plausible that transporters are involved either directly or indirectly in the underlying mechanism of hepatotoxicity. The interruption of biliary bile salt efflux has been reported as a cause for cholestatic liver damage (Pauli-Magnus & Meier, 2006) and inhibition of the bile salt export pump (BSEP) transporter by lapatinib and its phenol metabolite, M1, has recently been investigated (MacLauchlin et al., unpublished observations). Feng, et al. (2009), implicated a combination of direct cytotoxicity to mitochondria and inhibition of bile salt efflux to explain the clinical hepatotoxicity observed by a structurally similar tyrosine kinase inhibitor. In relation to both mechanisms of toxicity, the authors cite the role uptake and efflux transporters play in controlling intracellular hepatic concentrations.

This also may be an important factor to consider for lapatinib and its metabolites, especially considering the clinical doses (1250;1500 mg QD) when compared to the single 250 mg dose administered in this study and major dependence on hepatic metabolism for clearance and excretion.

Acknowledgements

The authors acknowledge Joe Polli, Cosette Serabjit-Singh, Chris Hunt, Rich Miller, Gordon Dear and Gary Boyle for valuable review and discussions.

Authorship Contribution

Participated in research design: Castellino, Koch; Bowers

Conducted experiments: Castellino, O'Mara; Borts

Performed data analysis: Castellino, O'Mara, Koch; Borts

Wrote or contributed to the writing of the manuscript: Castellino, Koch, Bowers; MacLauchlin

References

Bence AK, Anderson EB, Halepota MA, Doukas MA, DeSimone PA, Davis GA, Smith DA, Koch KM, Stead AG and Mangum S (2005) Phase I pharmacokinetic studies evaluating single and multiple doses of oral GW572016, a dual EGFR-ErbB2 inhibitor, in healthy subjects. *Invest New Drugs* **23**: 39-49.

Boyd B, Bozzo J, and Castaner J (2005) Lapatinib-oncolytic-dual EGFR and erbB-2 inhibitor. *Drugs Future* **30**(12): 1225-1239.

Chalasanni N and Bjornsson E (2010) Risk factors for idiosyncratic drug-induced liver injury. *Gastroenterology* **138**(7): 2246-2250.

Chessman D, Kostenko L, Lethborg T, Purcell AW, Williamson NA, Chen Z, Kjer-Nielsen L, Mifsud NA, Tait BD, Holdsworth R, Almeida CA, Nolan D, Macdonald WA, Archbold JK, Kellerher AD, Marriott D, Mallal S, Bharadwaj M, Rossjohn J and McCluskey J (2008) Human leukocyte antigen class I-restricted activation of CD8+ T cells provides the immunogenetic basis of a systemic drug hypersensitivity. *Immunity* **28**(6): 822-832.

Duckett DR and Cameron MD (2010) Metabolism considerations for kinase inhibitors in cancer treatment. *Expert Opin. Drug Metab. Toxicol.* **6**(10): 1175-1193.

Dalvie, DK, Kalgutkar AS, Khojasteh-Bakht SC, Obach, RS and O'Donnell JP (2002), Biotransformation reactions of five-membered aromatic heterocyclic rings. *Chem. Res. Toxicol.* **15**(3): 269-299.

Feng B, Xu JJ, Bi YA, Mireles R, Davidson R, Duignan DB, Campbell S, Kostrubsky VE, Dunn MC, Smith AR and Wang HF (2009) Role of hepatic transporters in the disposition and hepatotoxicity of a HER2 tyrosine kinase inhibitor CP-724,714. *Toxicological Sciences* **108**(2): 492–500.

Geyer CE, Forster J, Lindquist D, Chan S, Romieu CG, Pienkowski T, Jagiello-Gruszfeld A, Crown J, Chan A and Kaufman B (2006) Lapatinib plus capecitabine for HER2-positive advanced breast cancer. *N Engl J Med* **355**(26): 2733–2743.

Guengerich FP. (1999) Cytochrome P-450 3A4: regulation and role in drug metabolism. *Ann. Rev. Pharmacol. Toxicol.* **39**: 1-17.

GlaxoSmithKline, (2007) Tykerb product information. Available at

http://us.gsk.com/products/assets/us_tykerb.pdf

Johnston JB, Navaratnam S, Pitz MW, Maniate JM, Wiechec E, Baust H, Gingerich J, Skliris GP, Murphy LC, and Los M (2006) Targeting the EGFR pathway for cancer therapy. *Curr. Med. Chem.* **13**(29): 3483–3492.

Johnston SR and Leary A (2006) Lapatinib: a novel EGFR/HER2 tyrosine kinase inhibitor for cancer. *Drugs Today* **42**(7): 441–453.

Koch KM, Reddy NJ, Cohen RB, Lewis NL, Whitehead B, Mackay K, Stead A, Beelan AP and Lewis LD (2009) Effects of food on the relative bioavailability of lapatinib in cancer patients. *J. Clin. Oncol.* **27**(8): 1191-1196.

Kuo YH and Shih, KS (1991) A new method for preparation of 3-hydroxypyridines from furfurylamines in photooxygenation. *Chem. Pharm. Bull.* **39**(1): 181-183.

Loriot Y, Perlemuter G, Malka D, Penault-Llorca F, Boige V, Deutsch E, Massard C, Armand JP and Soria JC (2008) Drug insight: Gastrointestinal and hepatic adverse effects of molecular-targeted agents in chemotherapy. *Nat. Clin. Pract. Oncol.* **5**(5): 268-278.

Moy B and Goss PE (2006) Lapatinib: current status and future directions in breast cancer. *Oncologist* **11**(10): 1047–1057.

Moy B, Rappold E and Williams L (2009) Hepatobiliary abnormalities in patients with metastatic cancer treated with lapatinib. *J. Clin. Oncol.* ASCO Annual Meeting Proceedings (Post-Meeting Edition) **27**(15S): 1043.

Obach RS, Kalgutkar AS, Soglia JR and Zhao SX (2008) Can in vitro metabolism-dependent covalent binding data in liver microsomes distinguish hepatotoxic from

nonhepatotoxic drugs? An analysis of 18 drugs with consideration of intrinsic clearance and daily dose. *Chem. Res. Toxicol.* **21**(9): 1814-1822.

Parkin DM, Bray F, Ferlay J, and Pisani P (2005) Global cancer statistics, 2002. *CA Cancer J. Clin.* **55**(2): 74–108.

Park KB, Dalton-Brown E, Hirst C, and Williams DP (2006). Selection of new chemical entities with decreased potential for adverse drug reactions. *Eur J Pharmacol.* **549**(1-3):1–8.

Pauli-Magnus, C, and Meier PJ (2006). Hepatobiliary transporters and drug-induced cholestasis. *Hepatology* **44**(4): 778-787.

Polli JW, Humphreys JE, Harmon KA, Castellino S, O'Mara MJ, Olson KL, St. John-Williams LS, Koch KM and Serabjit-Singh CJ (2008) The role of efflux and uptake transporters in [N-{3-chloro-4-[(3-fluorobenzyl)oxy]phenyl}-6-[5-({[2-(methylsulfonyl)ethyl]amino}methyl)-2-furyl]-4-quinazolinamine (GW572016, lapatinib) disposition and drug interactions. *Drug Metab. Dispos.* **36**(4): 695-701.

Rodriguez RJ, Proteau PJ, Marquez BL, Hetherington CL, Buchholz CJ and O'Connell KL (1999) Flavin-containing monooxygenase-mediated metabolism of N-deacetyl ketoconazole by rat hepatic microsomes. *Drug Metabolism and Dispos.* **27**(8) 880-886.

Roffey SJ, Obach RS, Gedge JI and Smith DA, (2007) What is the objective of a mass balance study? A retrospective analysis of data in animal and human excretion studies employing radiolabeled drugs. *Drug Metabolism Reviews* **39**(1): 17-43.

Rowinsky EK (2004) The erbB family: targets for therapeutic development against cancer and therapeutic strategies using monoclonal antibodies and tyrosine kinase inhibitors. *Ann. Rev. Med.* **55**: 433–457.

Russman S, Jetter A and Kullak-Ublick GA (2010) Pharmacogenetics of drug-induced liver injury. *Hepatology* **52**(2): 748-761.

Smith DA, Koch KM, Arya N, Bowen CJ, Herendeen JM and Beelen A (2009) Effects of ketoconazole and carbamazepine on lapatinib pharmacokinetics in healthy subjects. *Br. J. Clin. Pharmacol.* **67**(4): 421-426.

Spraggs CF, Budde LR, Briley LP, Bing N, Cox CJ, King KS, Whittaker JC, Mooser VE, Preston AJ, Stein SH, and Cardon LR (2011) HLA-DQA1*02:01 is a major risk factor for lapatinib-induced hepatotoxicity in women with advanced breast cancer, *J. Clin. Oncol.* **29**(6): 667-673.

Takakusa H, Wahlin MD, Zhao C, Hanson KL, New LS, Chan EC and Nelson SD (2011) Metabolic intermediate complex formation of human cytochrome P450 3A4 by lapatinib. *Drug. Metab. Dispos.* **39**(6): 1022-1030.

Teng WC, Oh JW, New LS, Wahlin MD, Nelson SD, Ho HK and Chan, EC (2010)

Mechanism-based inactivation of cytochrome P450 3A4 by lapatinib. *Mol. Pharmacol.*

78(4): 693-703.

Shen DD, Kunze KL and Thummel KE (1997) Enzyme-catalyzed processes of first-pass

hepatic and intestinal drug extraction. *Adv. Drug Del. Rev.* **27**(2-3): 99-127.

Legends for Schemata and Figures

Scheme 1 N-oxidation cascade and α -carbon oxidation pathways

Scheme 2 Proposed enzymatic mechanism leading to the formation of hydroxypyridine metabolite (M2)

Scheme 3 Proposed photooxidation mechanism leading to the formation of the hydroxypyridine metabolite (M2)

Scheme 4 Possible lapatinib hepatotoxicity mechanisms

Figure 1: Chemical structure of [^{14}C]lapatinib (GW572016F) showing location of radiolabel

Figure 2: Concentration-Time Plot: Median (n=6) plasma concentrations of lapatinib (\circ , ng/ml) and total radioactivity (\bullet , ng/g)

Figure 3: Representative 4 hour pooled plasma extract HPLC-radiochemical chromatogram from healthy subjects following a single oral administration of [^{14}C]-lapatinib (250 mg)

Figure 4: A composite of extracted ion chromatograms (EIC) obtained from the LC/MS analysis of pooled human plasma (female subject, =1.5 to 6 hours)

Figure 5: Representative HPLC-radiochemical chromatograms of fecal homogenate extracts from healthy subjects following a single oral administration of [^{14}C]-lapatinib (250 mg)

Figure 6: MS fragmentation of lapatinib

Table 1. Median (range) Pharmacokinetic Parameters (n=6)

Parameter (units)	Lapatinib	Total Radioactivity	Ratio
C _{max} (mg/L)	0.33 (0.15-1.07)	0.72 (0.40-1.69)	----
T _{max} (h)	4.05 (2.53-5.97)	4.03 (3.03-5.97)	----
AUC _∞ (h.mg/L)	3.58 (2.31-13.0)	6.79 (4.51-23.0)	0.54 (0.47-0.57)
t _{1/2} (h)	14.8 (11.5-20.5)	5.59 ¹ (4.50-14.6)	----
Urinary recovery (% of dose)	----	1.15 (0.49-1.61)	----
Fecal recovery (% of dose)	27.0 (2.68-66.9)	91.7 (60.3-98.3)	0.33 (0.04-0.72)
Total recovery (% of dose)	----	93.0 (61.6-99.7)	----

¹Value likely underestimated due to detection limits for radioactivity.

Table 2. Median excretion balance results by sex (% dose)

Subjects	Urine	Feces	Total
All subjects (n=6)	1.2	91.8	93.0
Male (n=3)	1.0	93.6	94.6
Female (n=3)	1.3	89.9	91.5

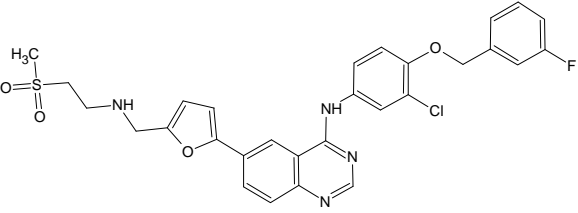
Median data are shown due to variability in recovery of total radioactivity.

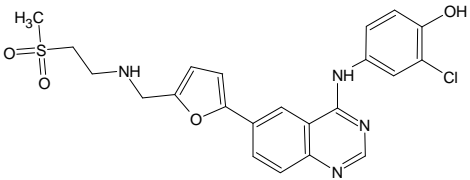
Table 3. Median percentage of cumulative radioactivity recovered from six healthy male and female subjects after a single 250 mg oral suspension dose of [14C]-lapatinib

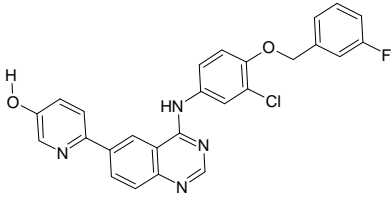
Time Period	Feces	Urine	Total
h	% dose	% dose	% dose
0-24	10.5	1.01	
0-48	45.3	1.16	
0-72	74.9	1.16	
0-96	78.4	1.16	
0-120	90.8	1.16	
0-144	91.4	1.16	
0-168	91.8	1.16	93.1

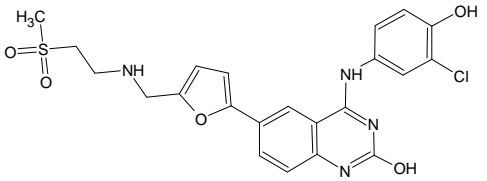
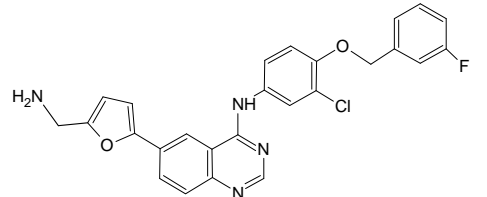
Median data are shown due to variability in recovery of total radioactivity.

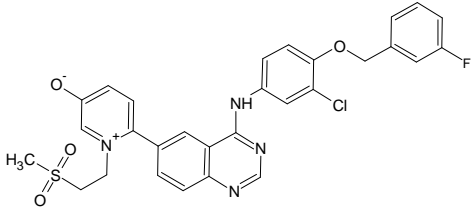
Table 4. Analytical Reference Data for Lapatinib and metabolites

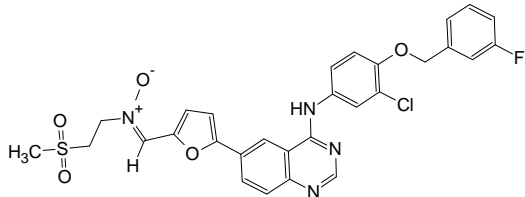
Proposed Structure	$[M+H]^+$ (m/z)	Characteristic Fragment Ions (m/z)	1H -NMR (600 MHz)
 <p style="text-align: center;">Lapatinib (GW572016)</p>	581	458, 393, 379, 365, 350	1H NMR (D ₂ O: ACN) δ ppm 3.05 (s, 3 H) 3.54(m, 2 H) 3.58 (m, 2 H) 4.40 (s, 2 H) 5.20 (s, 2 H) 6.80 (d, $J=3.43$ Hz, 1 H) 7.08 (d, $J=3.43$ Hz, 1 H) 7.08 - 7.11 (m, 1 H) 7.21 (d, $J=8.88$ Hz, 1 H) 7.20 - 7.24 (m, 1 H) 7.28 (d, $J=7.47$ Hz, 1 H) 7.40 (dq, 1 H) 7.48 (dd, $J=8.95, 2.57$ Hz, 1 H) 7.74 (d, $J=2.65$ Hz, 1 H) 7.84 (d, $J=8.56$ Hz, 1 H) 8.35 (dd, $J=8.72,$ 1.71 Hz, 1 H) 8.60 (s, 1 H) 8.76 (d, $J=1.40$ Hz, 1 H

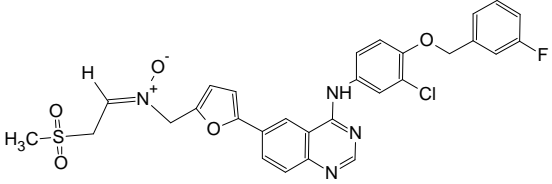
Proposed Structure	$[M+H]^+$ (m/z)	Characteristic Fragment Ions (m/z)	1H -NMR (600 MHz)
 <p style="text-align: center;">M1</p>	473	393, 379, 367, 351, 350	1H NMR (DMSO- d_6) δ ppm 3.03 (s, 3 H) 3.01 - 3.07 (m, 2 H) 3.27 - 3.35 (m, 2 H) 3.86 - 3.92 (br s, 2 H) 6.51 (br. d, $J=2.80$ Hz, 1 H) 7.00 (d, $J=8.72$ Hz, 1 H) 7.06 (d, $J=3.11$ Hz, 1 H) 7.14 (br s, 1 H) 7.57 (dd, $J=8.72, 2.49$ Hz, 1 H) 7.77 (d, $J=8.72$ Hz, 1 H) 7.86 (d, $J=2.49$ Hz, 1 H) 8.13 (dd, $J=8.72, 1.56$ Hz, 1 H) 8.50 (s, 1 H) 8.78 (d, $J=1.87$ Hz, 1 H) 9.85 (br s, 1 H) 10.06 (br s, 1 H)

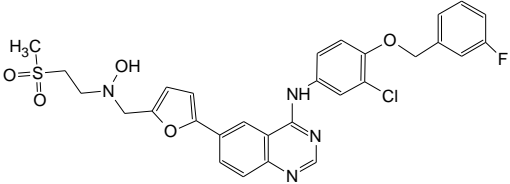
Proposed Structure	$[M+H]^+$ (m/z)	Characteristic Fragment Ions (m/z)	$^1\text{H-NMR}$ (600 MHz)
 <p style="text-align: center;">M2</p>	473	364, 363, 336, 335, 329, 301	$^1\text{H NMR}$ (DMSO- d_6) δ ppm 5.26 (s, 2 H) 7.15 - 7.20 (m, 1 H) 7.24 - 7.27 (m, 1 H) 7.28 (d, $J=9.34$ Hz, 1 H) 7.30 - 7.32 (m, 1 H) 7.33 (m, $J=6.85$ Hz, 1 H) 7.35 (dd, $J=8.20, 2.80$ Hz, 1 H) 7.76 (dd, $J=9.01, 2.50$ Hz, 1 H) 7.82 (d, $J=8.72$ Hz, 1 H) 8.02 (d, $J=2.49$ Hz, 1 H) 8.04 (d, $J=8.72$ Hz, 1 H) 8.30 (d, $J=3.11$ Hz, 1 H) 8.50 (dd, $J=8.88, 1.71$ Hz, 1 H) 8.56 (s, 1 H)

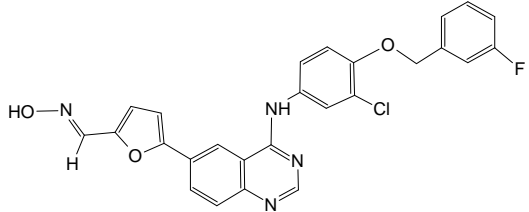
Proposed Structure	$[M+H]^+$ (m/z)	Characteristic Fragment Ions (m/z)	$^1\text{H-NMR}$ (600 MHz)
 <p style="text-align: center;">M3</p>	489	366, 323	$^1\text{H NMR}$ (600 MHz, DMSO- d_6) δ ppm 2.96 (t, $J=6.80$ Hz, 2H) 3.01 (s, 3 H) 3.25 (t, $J=6.80$ Hz, 2 H) 3.78 (s, 2 H) 6.41 (d, $J=3.11$ Hz, 1 H) 6.83 (d, $J=3.11$ Hz, 1 H) 7.00 (d, $J=8.72$ Hz, 1 H) 7.20 (d, $J=8.41$ Hz, 1 H) 7.50 (dd, $J=8.72, 2.18$ Hz, 1 H) 7.83 (d, $J=2.18$ Hz, 1 H) 7.90 (dd, $J=8.72, 1.24$ Hz, 1 H) 8.53 (s, 1 H) 9.73 (s, 1 H)
 <p style="text-align: center;">M4</p>	475	366, 365	Not Acquired (Authentic Standard Available)

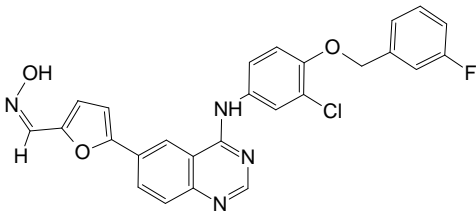
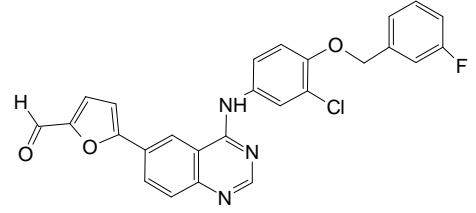
Proposed Structure	$[M+H]^+$ (m/z)	Characteristic Fragment Ions (m/z)	$^1\text{H-NMR}$ (600 MHz)
 <p style="text-align: center;">M5</p>	579	470, 391, 363, 327, 263	$^1\text{H NMR}$ (600 MHz, $\text{DMSO-}d_6$) δ ppm 2.97 (s, 3 H) 3.88 (t, 2 H) 4.98 (t, $J=7.03$ Hz, 2 H) 5.27 (s, 2 H) 7.15 - 7.20 (m, 1 H) 7.30 (m, 1 H) 7.31 (d, $J=9.24$ Hz, 1 H) 7.32 - 7.34 (m, 1 H) 7.44 - 7.48 (m, 1 H) 7.80 (dd, $J=8.83, 2.41$ Hz, 1 H) 8.04 (d, $J=8.84$ Hz, 1 H) 8.07 (d, $J=8.23$ Hz, 1 H) 8.07 (d, $J=2.61$ Hz, 1 H) 8.16 (dd, $J=8.63, 1.00$ Hz, 1 H) 8.26 (dd, $J=8.83, 2.41$ Hz, 1 H) 8.86 (br s, 1 H) 8.95 (d, $J=2.61$ Hz, 1 H) 9.37 (br s, 1 H)

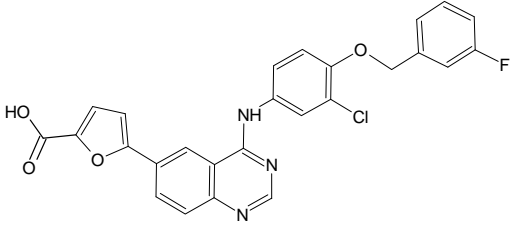
Proposed Structure	$[M+H]^+$ (m/z)	Characteristic Fragment Ions (m/z)	$^1\text{H-NMR}$ (600 MHz)
 <p style="text-align: center;">M6 ($\Delta\text{N}_7\text{-C}_6\text{- Nitronium}$)</p>	595	489, 471, 380, 363, 350	$^1\text{H NMR}$ (DMSO- d_6) δ ppm 3.05 (s, 3 H) 3.75 (t, $J=6.23$ Hz, 2 H) 4.43 (t, $J=6.54$ Hz, 2 H) 5.26 (s, 2H) 7.18 (td, $J=8.70, 2.60$ Hz, 1 H) 7.29 (d, $J=9.03$ Hz, 1 H) 7.30 (m, 1 H) 7.32 (d, $J=3.74$ Hz, 1 H) 7.33 (d, $J=8.72$ Hz, 1 H) 7.45 - 7.49 (m, 1 H) 7.76 (dd, $J=8.82, 2.61$ Hz, 1 H) 7.81 (d, $J=3.43$ Hz, 1 H) 7.83 (d, $J=8.72$ Hz, 1 H) 8.03 (d, $J=2.49$ Hz, 1 H) 8.22 (dd, $J=8.41, 1.56$ Hz, 1 H) 8.28 (~s, 1 H) 8.58 (s, 1 H) 8.86 (d, $J=1.56$ Hz, 1 H) 9.97 (s, 1 H) Stereochemistry of nitronium set by NOE

Proposed Structure	$[M+H]^+$ (m/z)	Characteristic Fragment Ions (m/z)	$^1\text{H-NMR}$ (600 MHz)
 <p style="text-align: center;">M7 ΔN₇-C₈- Nitron</p>	595	489, 471, 380, 363, 350	Unstable during isolation

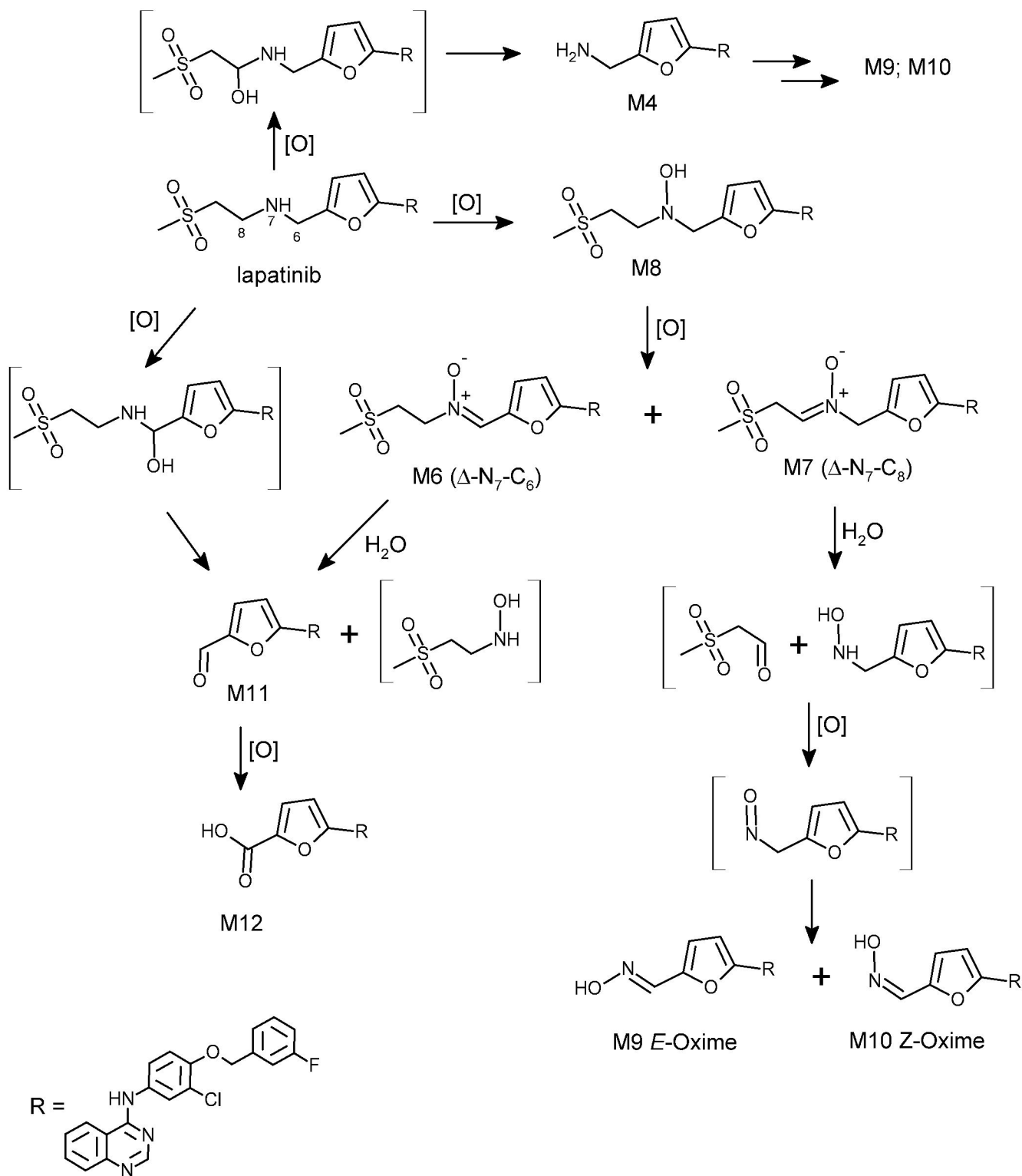
Proposed Structure	$[M+H]^+$ (m/z)	Characteristic Fragment Ions (m/z)	$^1\text{H-NMR}$ (600 MHz)
 <p style="text-align: center;">M8</p>	597	491, 459, 382, 364, 350, 335, 306	$^1\text{H NMR LC-NMR}$ (D_2O : ACN) δ ppm 3.00 (s, 3 H) 3.17 (br t, $J \approx 7$ Hz, 2 H) 3.39 (br t, $J = 6.77$ Hz, 2H) 3.99 (s, 2 H) 5.23 (s, 2 H) 6.53 (d, $J = 3.43$ Hz, 1 H) 7.02 (d, $J = 3.43$ Hz, 1 H) 7.06 - 7.11 (m, 1 H) 7.20 (d, $J = 9.03$ Hz, 1 H) 7.20 - 7.25 (m, 1 H) 7.28 (d, $J = 7.32$ Hz, 1 H) 7.37 - 7.43 (m, 1 H) 7.50 (dd, $J = 8.64, 2.73$ Hz, 1 H) 7.76 (d, $J = 2.49$ Hz, 1 H) 7.82 (d, $J = 8.72$ Hz, 1 H) 8.32 (dd, $J = 8.56, 1.71$ Hz, 1 H) 8.58 (s, 1 H) 8.70 - 8.72 (m, 1 H)

Proposed Structure	$[M+H]^+$ (m/z)	Characteristic Fragment Ions (m/z)	$^1\text{H-NMR}$ (600 MHz)
 <p style="text-align: center;">M9 <i>E</i>-Oxime</p>	489	380, 363, 350	$^1\text{H NMR LC-NMR}$ (D_2O : ACN) δ ppm 5.23 (s, 2 H) 6.87 (d, $J=3.74$ Hz, 1 H) 7.06 - 7.11 (m, 1 H) 7.14 (d, $J=3.43$ Hz, 1 H) 7.21 (d, $J=8.72$ Hz, 1 H) 7.21 - 7.24 (m, 1 H) 7.27 - 7.29 (m, 1 H) 7.38 - 7.43 (m, 1 H) 7.52 (dd, $J=8.72, 2.49$ Hz, 1 H) 7.79 (d, $J=2.18$ Hz, 1 H) 7.84 (d, $J=8.72$ Hz, 1 H) 8.07 (s, 1 H) 8.38 (dd, $J=8.72, 1.56$ Hz, 1 H) 8.60 (s, 1 H) 8.84 (d, $J=2.18$ Hz, 1 H)

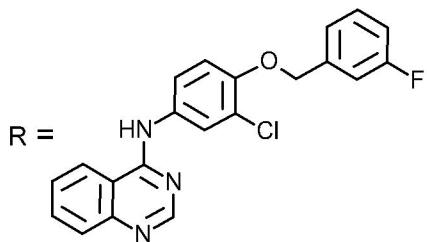
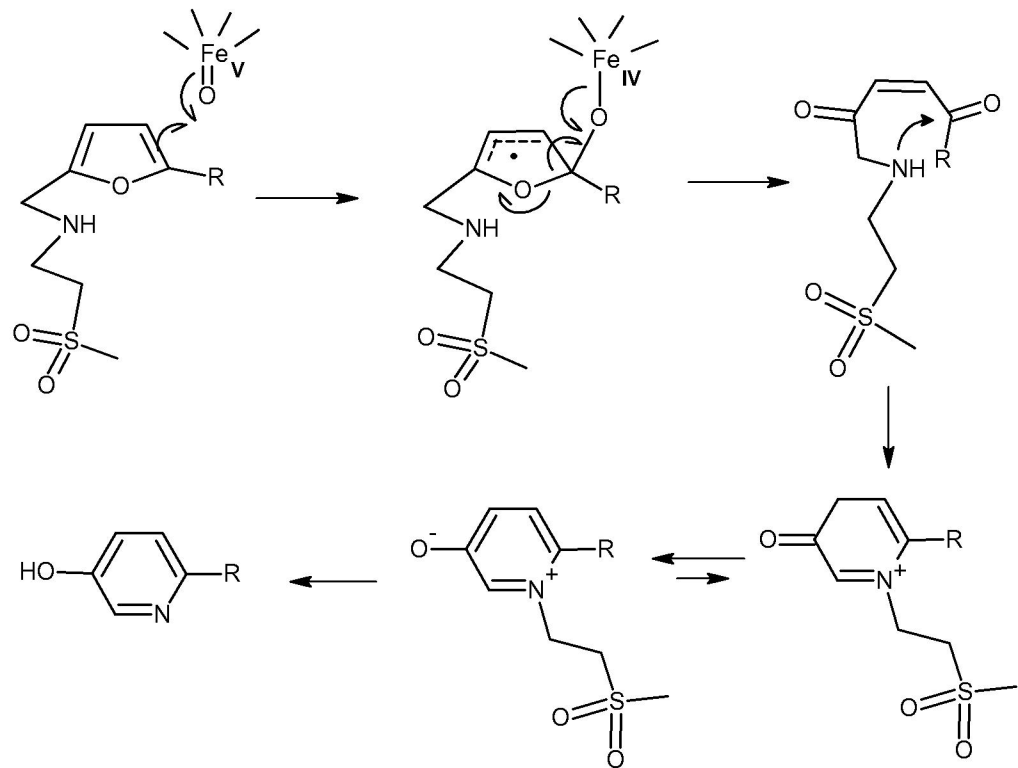
Proposed Structure	$[M+H]^+$ (m/z)	Characteristic Fragment Ions (m/z)	$^1\text{H-NMR}$ (600 MHz)
 <p style="text-align: center;">M10 Z-Oxime</p>	489	380, 363, 350	$^1\text{H NMR LC-NMR}$ (D_2O : ACN) δ ppm 5.23 (s, 2 H) 7.05 - 7.10 (m, 1 H) 7.20 (d, $J=8.57$ Hz, 1 H) 7.20 (d, $J=3.43$ Hz, 1 H) 7.20 - 7.23 (m, 1 H) 7.27 (m, $J=7.40$, 1.48 Hz, 1 H) 7.38 - 7.42 (m, 1 H) 7.41 (d, $J=3.74$ Hz, 1 H) 7.50 (dd, $J=8.80$, 2.73 Hz, 1 H) 7.60 (s, 1 H) 7.76 (d, $J=2.49$ Hz, 1 H) 7.84 (d, $J=9.19$ Hz, 1 H) 8.38 (dd, $J=8.64$, 1.48 Hz, 1 H) 8.59 (s, 1 H) 8.82 (d, $J=2.18$ Hz, 1 H)
 <p style="text-align: center;">M11</p>	474	337, 309	Not Acquired (Authentic Standard Available)

Proposed Structure	[M+H]⁺ (m/z)	Characteristic Fragment Ions (m/z)	¹H-NMR (600 MHz)
 <p>M12</p>	490	381, 337, 309	Not Acquired (Authentic Standard Available)

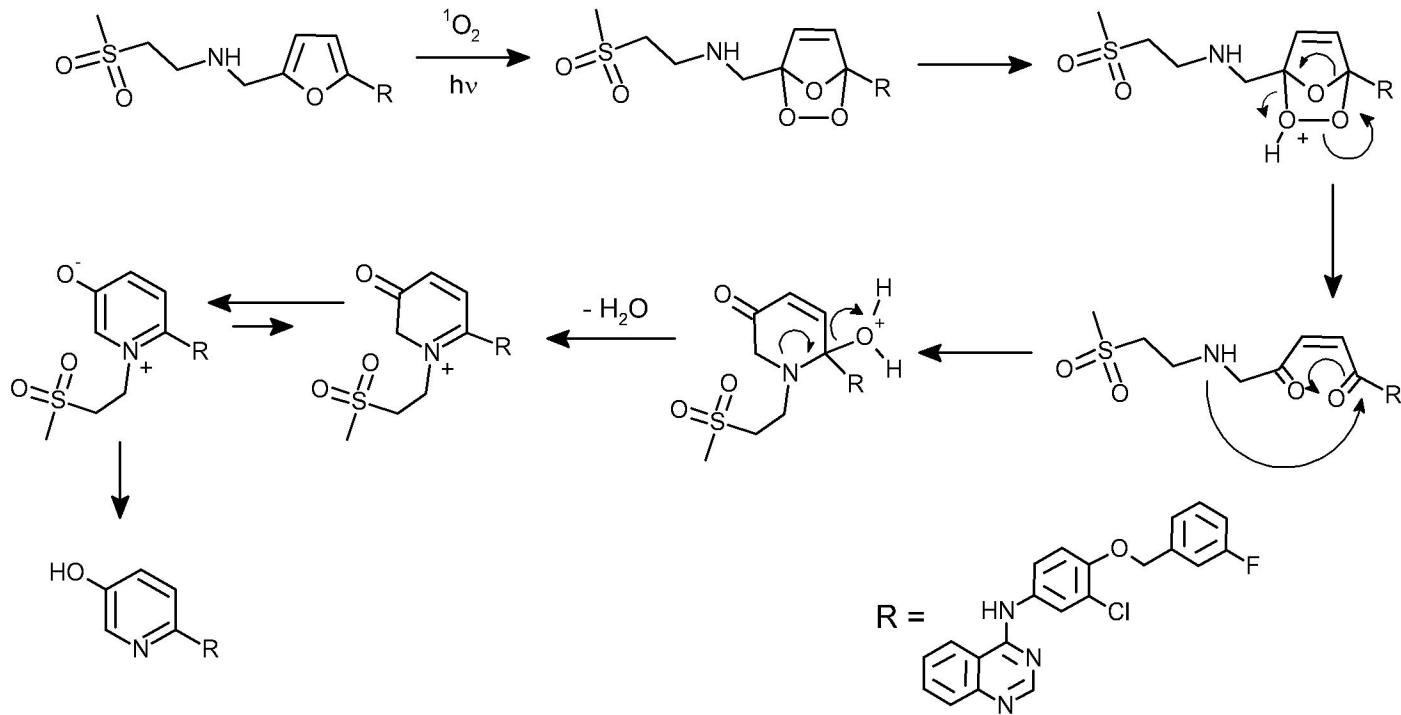
Scheme 1



Scheme 2



Scheme 3



Scheme 4

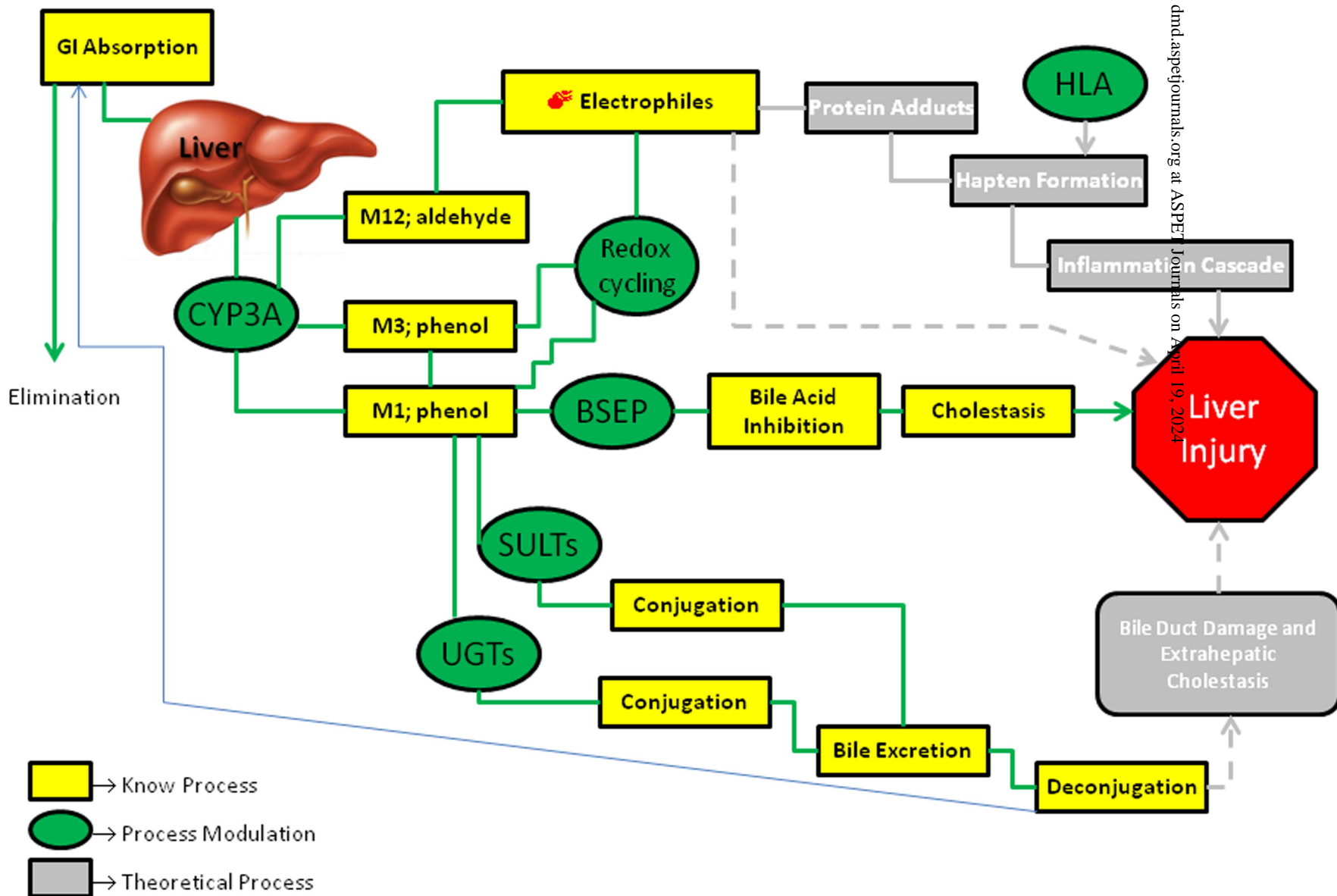


Figure 1

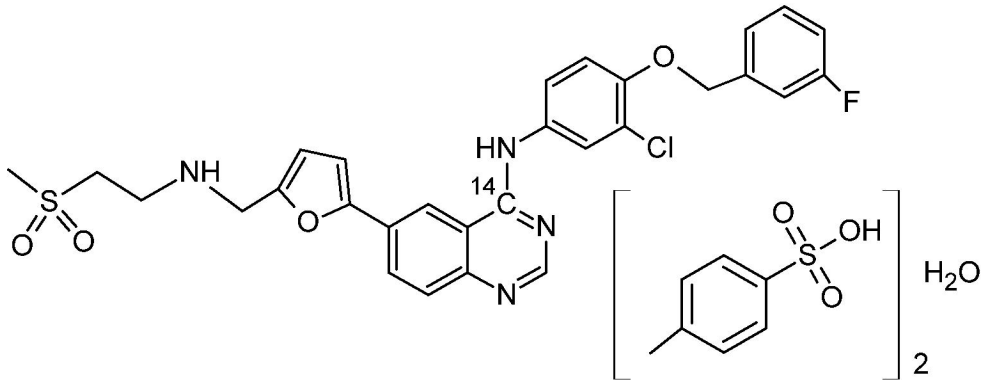


Figure 2

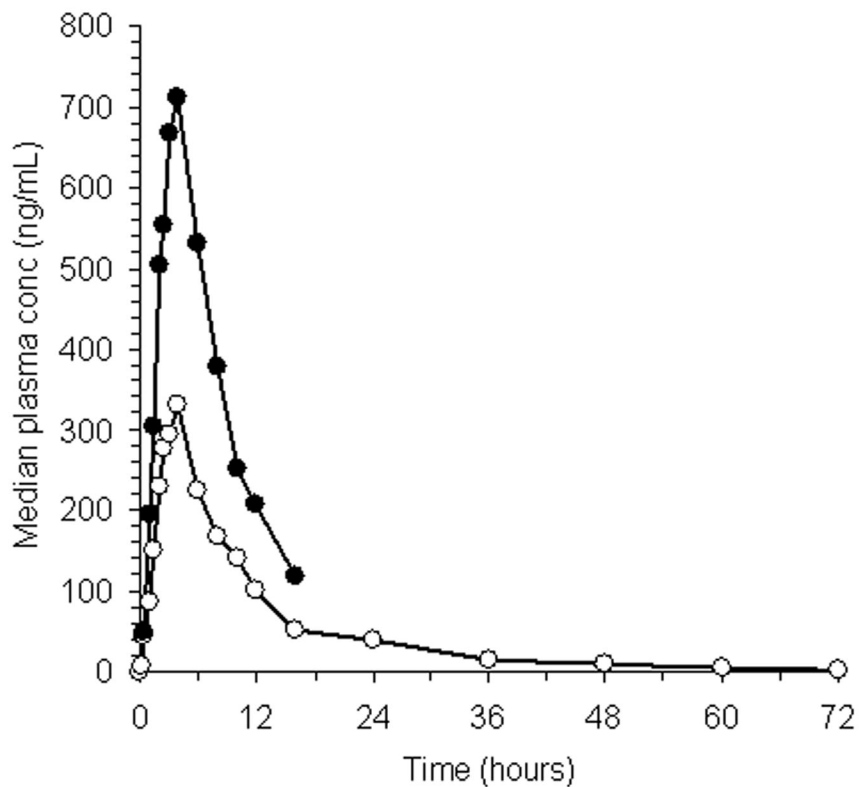


Figure 3

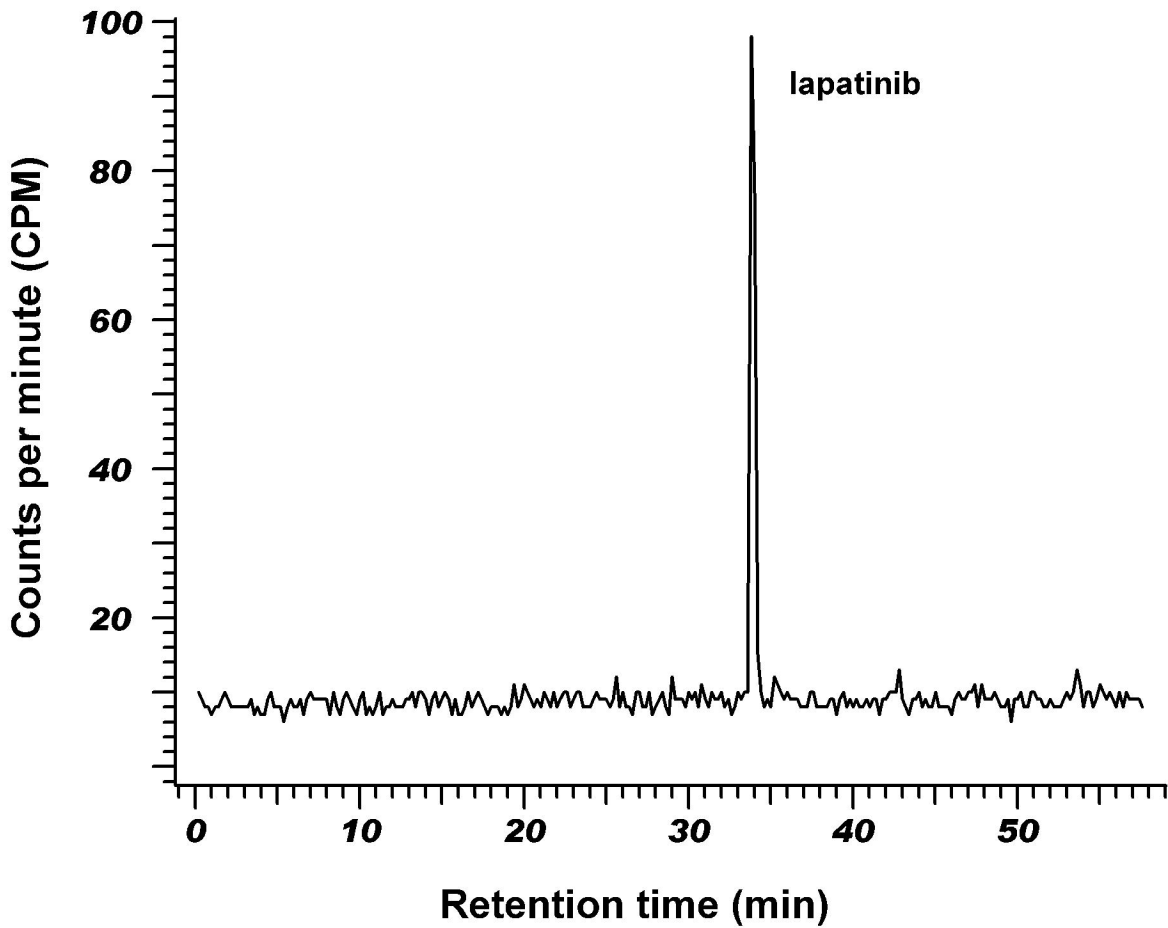


Figure 4

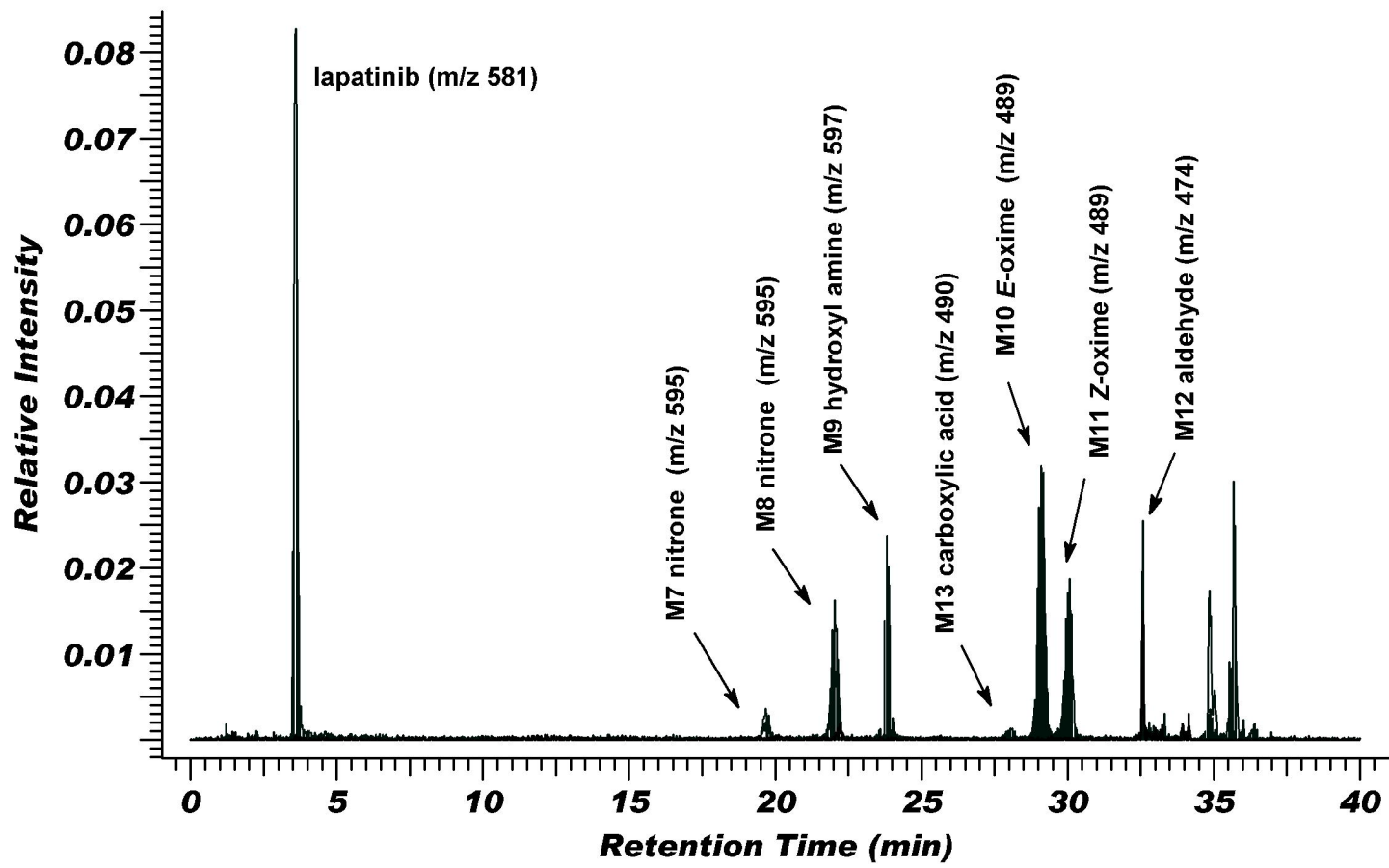


Figure 5

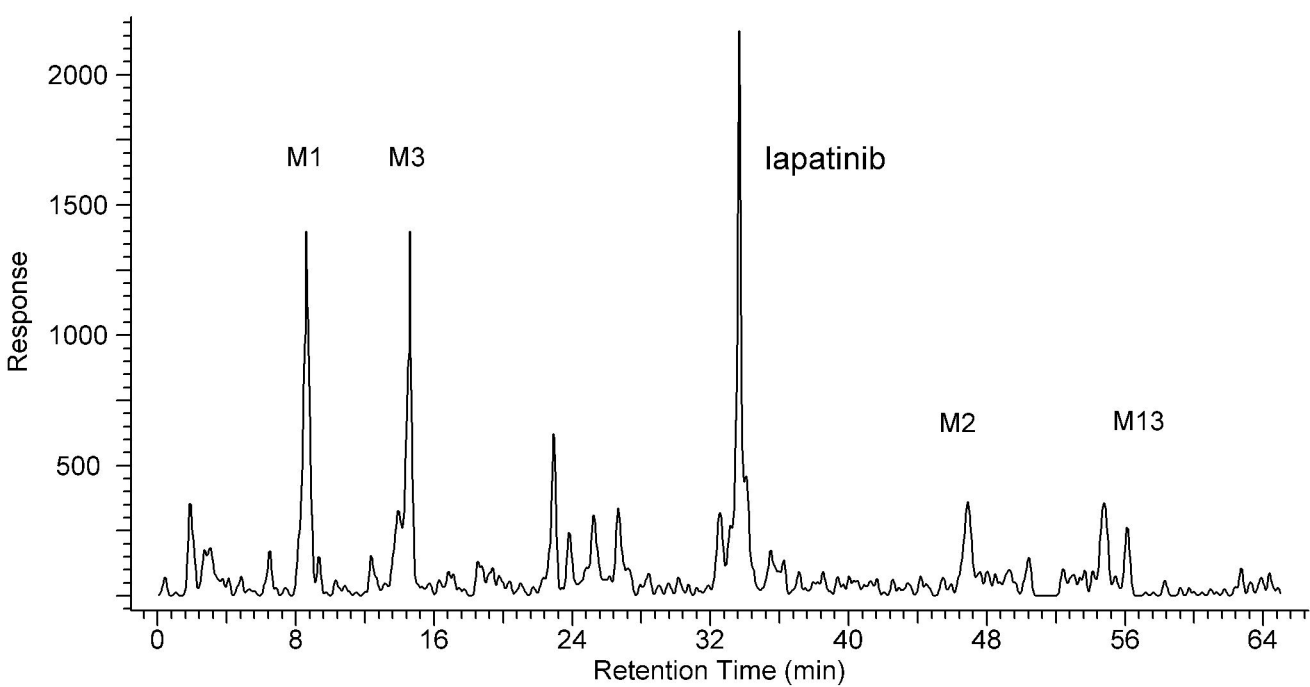
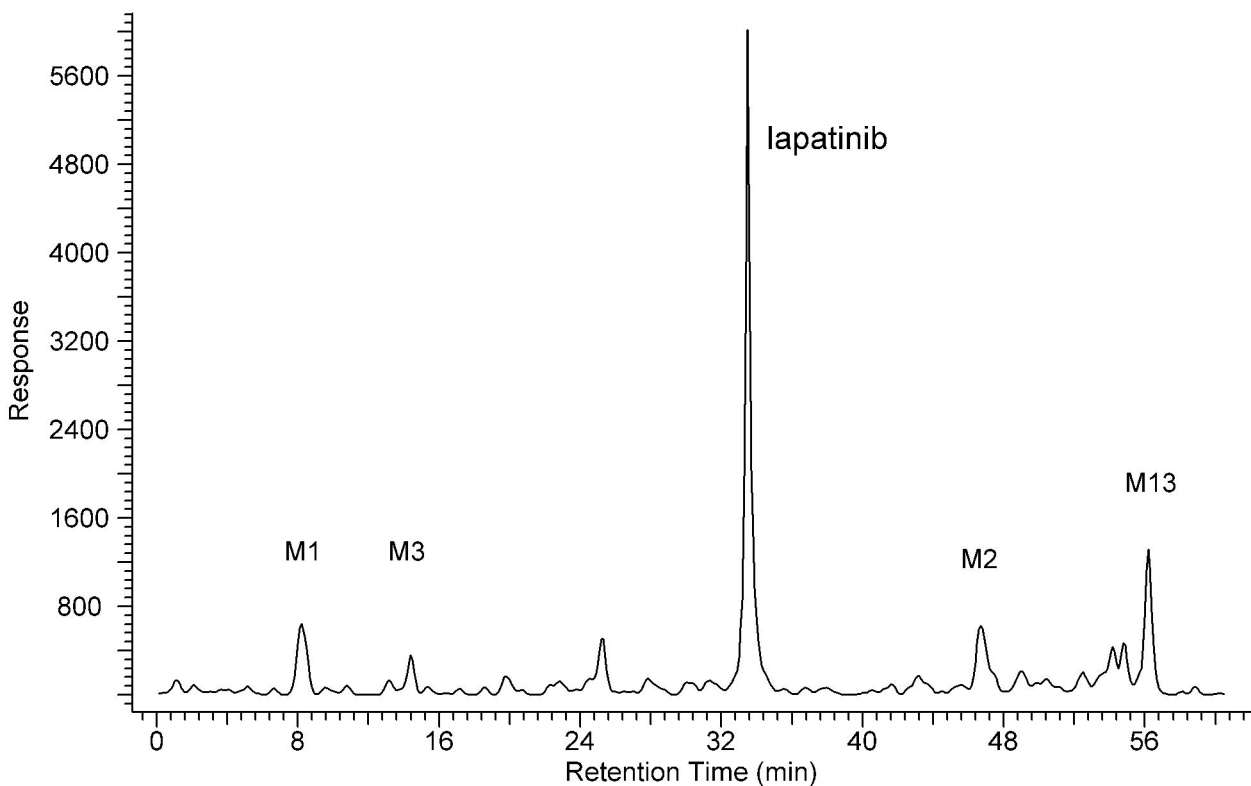


Figure 6

